Journal Pre-proofs

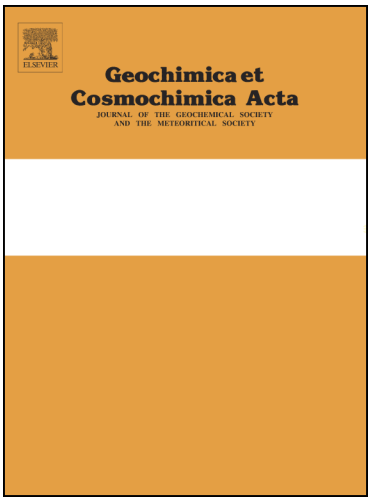

Quantification of sulphide oxidation rates in marine sediment

Alyssa J. Findlay, André Pellerin, Katja Laufer, Bo Barker Jørgensen

PII: S0016-7037(20)30234-9
DOI: https://doi.org/10.1016/j.gca.2020.04.007
Reference: GCA 11730

To appear in: *Geochimica et Cosmochimica Acta*

Received Date: 5 April 2019
Revised Date: 4 April 2020
Accepted Date: 6 April 2020

Please cite this article as: Findlay, A.J., Pellerin, A., Laufer, K., Barker Jørgensen, B., Quantification of sulphide oxidation rates in marine sediment, *Geochimica et Cosmochimica Acta* (2020), doi: https://doi.org/10.1016/j.gca.2020.04.007

Quantification of sulphide oxidation rates in marine sediment

Alyssa J. Findlay[1]*†, André Pellerin[1]*, Katja Laufer[1,2], Bo Barker Jørgensen[1]

[1]Center for Geomicrobiology and Section for Microbiology, Department of Bioscience, Aarhus University, Denmark

[2] GEOMAR Helmholtz Centre for Ocean Research Kiel, Germany

*Co-first author

†Corresponding author, afindlay@bios.au.dk

Abstract

The marine sulphur cycle is driven by the reduction of sulphate to sulphide coupled to microbial decomposition of organic matter. The sulphide produced by sulphate reduction may either react with Fe or organic matter to be buried as pyrite or organic sulphur, respectively; or may be oxidised through different pathways and intermediates. The amount of sulphide that is oxidised in marine sediments is not well constrained, yet oxidative sulphur cycling has critical implications for hypoxic coastal waters and oxygen minimum zones, carbon mineralisation, microbial metabolism and the interpretation of ancient and modern stable isotope signatures. Here, we present an experimental method to directly determine sulphide oxidation rates in undiluted marine sediment incubations. We find that sulphide oxidation rates in the top two centimetres of organic-rich coastal sediments were greater than rates of sulphide production through sulphate reduction and calculate that in the top 6 centimetres, up to 92 % of sulphide produced during sulphate reduction was reoxidised. The rates decreased steeply with depth, however, and sulphide oxidation to sulphate could no longer be quantified 10 cm below the seafloor. Fe oxides were the primary oxidant for sulphide and the sulphide oxidation rate was related to the amount and reactivity of the Fe minerals. These results provide important insights into the magnitude and processes of the sulphur cycle in marine sediments.

1. Introduction

The partitioning of carbon between different reservoirs (sediments, oceans, atmosphere) is closely linked with the development of Earth's climate and redox state (Lyons et al., 2014). Organic carbon deposited on the seafloor drives diagenetic processes through decomposition coupled to a sequence of electron acceptors (O_2>NO_3^->MnO_2>FeOOH>SO_4^{2-}> CO_2) based on free energy yield (Froelich et al., 1979). Although less energetically favourable than oxidation by oxygen, nitrate, manganese, or iron oxides, microbial sulphate reduction (MSR) to sulphide is a key process for the remineralisation of organic matter due to the high concentrations of sulphate in seawater relative to other potential oxidants.

Mass balance calculations have indicated that only 5-20 % of the sulphide produced via MSR is buried as pyrite in continental shelf sediments (Jørgensen et al., 1990); therefore

the majority must be cycled within the sediment. The oxidation of sulphide back to sulphate proceeds through a web of chemical and biological pathways and results in a variety of species with intermediate oxidation states (S_x^{2-}, S^0, $S_2O_3^{2-}$, $S_4O_6^{2-}$, SO_3^{2-}) that can themselves be oxidised, reduced, or disproportionated (e.g., Findlay and Kamyshny, 2017).

This sedimentary sulphur cycle has extensive biogeochemical importance. Sulphide oxidation represents a major sink for oxygen in sediments (Jørgensen, 1982). Particularly in hypoxic and anoxic systems, diffusion of sulphide from the sediment is the main source of sulphide to the water column, where it can cause environmental problems such as fish kills (Luther et al., 2004). The net balance between sulphate reduction, sulphur burial and sulphide oxidation also affects alkalinity, which in turn influences the capacity of a system to take up CO_2 (Wurgarft et al., *Accepted*; Brenner et al., 2016). Sulphide and its oxidation intermediates are used by a variety of microorganisms for energy conservation (Thamdrup et al., 1993; Finster, 2008). Reduced sulphur compounds (H_2S, S_x^{2-}, S^0) react with buried iron minerals to form pyrite (Rickard and Luther, 2007), the largest sink for sulphur from the world's oceans (Fike et al., 2013), and may also react with organic matter to be buried as organic sulphur (Brüchert, 1998; Raven et al., 2016). The relative ratio of sulphur burial as pyrite, organic matter burial and the oxidation of these two pools controls atmospheric O_2 concentrations over geological timescales (Berner et al., 2000). Furthermore, the sulphur isotopic signature of pyrite conserved throughout the rock record is used extensively to reconstruct the paleo-redox conditions of the Earth's atmosphere and oceans (Habicht et al., 2002; Bottrell and Newton, 2006; Johnston, 2011; Jamieson et al., 2013).

Understanding the magnitude of the sedimentary sulphur cycle, including sulphide oxidation, is thus of critical importance for estimates of past and present element fluxes and burial, microbial metabolism and carbon budgets. Despite this, oxidative sulphur cycling in sediments is not well constrained. Most sulphide oxidation occurs anaerobically (Jørgensen and Nelson, 2004), and is evidenced by the presence of elemental sulphur within the surface sediment (Troelsen and Jørgensen, 1982; Henneke et al., 1997; Zopfi et al., 2004; Yücel et al., 2010). Lower amounts of oxidation have also been recently demonstrated in deeper sediments, extending below the sulphate-methane transition zone (SMTZ) (Holmkvist et al., 2014; Pellerin et al., 2018).

The large number and reactivity of sulphide oxidation intermediates makes rate and pathway determinations by mass balance alone difficult. Nonetheless, sulphide oxidation in sediments has been studied extensively through oxidant amendments (Burdige and Nealson, 1986; Aller and Rude, 1988; Canfield, 1989), the characterisation of Fe oxide pools (Canfield et al., 1992) and radiotracer experiments (King, 1990; Fossing et al., 1992). These radiotracer experiments, using injections of $H_2{}^{35}S$ or $^{35}S^0$, were applied to the study of reduced sulphur transformations, but their applicability was limited due to the discovery of rapid isotope exchange of ^{35}S among the reduced sulphur pool (ΣH_2S, FeS, S_x^{2-} and S^0) (Fossing and Jørgensen, 1990; King, 1990; Fossing et al., 1992). Despite this limitation, these experiments were able to qualitatively demonstrate the oxidation of sulphide in natural sediments.

Here, this experimental method has been further developed using amendment of radioactive sulphide in order to obtain quantitative measurements of sulphide oxidation rates to sulphate concurrent to sulphate reduction in undiluted sediment incubations. The method and experimental design are presented, as well as sulphide oxidation rate profiles from organic-rich, sulfidic sediment. These are the first direct measurements of sulphide oxidation rates in sediments and thus provide important insights into the quantitative importance of sulphur cycling in marine sediment.

2. Methodology

2.1 Incubation experiments

Sediment cores (Core A, 70 cm long and Core B, 30 cm long) were taken in November 2017 and February 2018, respectively, from Station M5 (56°06.20 N and 10°27.47 E; water depth 28 m). A third core from the same station was used for the Fe extractions. Station M5 is located in Aarhus Bay, a shallow basin with high organic matter input and sulphur and iron cycling, as documented through multiple publications. Thus, the distribution of sulphate reduction and sulphate reducing bacteria in the near-surface sediment was recently determined at high depth resolution for this site (Jochum et al., 2017; Petro et al., 2019; Beulig et al.,2019), while sulphur, iron and manganese transformations were quantified by Thamdrup et al. (1994) and Holmkvist et al. (2011). Further relevant studies were done of sedimentation rates and sediment mixing (Chen et al., 2017), organic matter geochemistry (Langerhuus et al., 2012; Glombitza et al., 2014), and iron cycling bacteria (Laufer et al., 2016)

The cores were maintained at *in situ* temperature until use in experiments, typically 1-2 weeks after sample collection. Incubation experiments were set up from collected and sectioned sediment cores as bag incubations in gas-tight plastic bags (Escal Neo, high gas barrier bag, Mitsubishi Gas Chemical Co., Inc.) in order to allow homogenisation of the sediment without the dilution, gas space, or other disturbances that are generally associated with slurry experiments and that have been shown to enhance rates of sulphate reduction relative to undisturbed sediment in whole-core incubations (Hansen et al., 2000). However, any homogenisation procedure disturbs the sediments and may change the actual rates, either due to activation of organic material or, in this case, perhaps to activation of Fe oxide surfaces. Since the concentration of sulphide in the experiments does not change from the very start of the experiment through the first ca. 24 hours, we assume that any error introduced by this effect is small compared to the other sources of error in the experiments (for example due to differences in solid phase S concentrations due to sediment heterogeneity, which were about 20%). In order to limit the potential for oxidation artefacts, the experiments and all sub-sampling were conducted in a glove bag under an anoxic atmosphere purged three times and then filled with N_2 gas. Bags contained 200-300 g of sediment. Incubation experiments were started by injecting about 400 MBq $H_2{}^{35}S$ formed from reduction of $^{35}SO_4{}^2$ (NEX041, Perkin-Elmer) via the STRIP method (Arnold et al., 2014) and non-radioactive SO_4^{2-} (8 mg Na_2SO_4). The H_2S gas evolved during the distillation was trapped in trace metal free NaOH (Wu and Boyle 1998). We note that, despite these precautions, a small amount of sulphide tracer likely oxidised, as indicated by the high background sulphate radioactivity at the start of the experiments. The radioactive sulfide solution was used immediately because an increase in the activity of the sulfate became measurable in the stock tracer (5% after 24 hours). Thus, fresh tracer was prepared whenever a new incubation was started. One injection of 5 mL of undilted tracer was then added to 500 mL of sediment. Due to isotope exchange between porewater sulphide and solid-phase S^0 and AVS, proper homogenisation of the solid sediment was critical. Homogenisation was carried out in a gas-tight bag after the addition of the radioactive tracer using a whisk. In order to ensure that our homogenization technique was reliable, we practiced by homogenizing food coloring into a mixture of flour and whipped cream made to resemble the consistency of our sediment. This allowed us to understand the timescale needed for proper homogenization as well as the identification of dead spots within the bag which were prone to under-mixing (the corners). The sediment was then mixed in this manner for 10 minutes in order to ensure complete homogenisation. Care was taken to ensure that homogenization of the tracer would be effective by ensuring that all of the sediment was

continuously mixed including the corners of the bag. Sampling a bag in three different areas of the bag after homogenization showed the same level of radioactivity, indicating efficient homogenization. We note that other homogenisation techniques, such as kneading the bag e.g. (Hansen et al., 2000), did not produce sufficient homogeneity in the solid-phase for reproducible, quantitative measurements. Following injection of the tracer and homogenisation, subsamples were taken over time to determine the concentration and radioactivity of the different sulphur pools.

In order to account for the specific radioactivity of all major sulphur species, the sulphur pools were separated in each subsample through the following procedure (illustrated in Fig. 1). First, the subsample was centrifuged in the glovebag in order to separate the porewater from the solid-phase. The porewater was decanted, sulphide was precipitated as ZnS and the porewater sample was centrifuged again. The radioactivity in the supernatant was measured and attributed to radioactivity in SO_4^{2-}. We note that it is not possible to separate the other oxyanions here, but significant radioactivity cannot accumulate in these pools, as the concentrations are very low (hundreds of nanomolar, Thamdrup et al., 1994b). In order to ensure that only the radioactivity in sulphide was measured (and not trace amounts of radioactivity in sulphate), the ZnS precipitate was distilled in HCl (6 M) with non-radioactive carrier (ZnS), trapped again as ZnS and the radioactivity was measured, accounting for radioactivity in porewater H_2S. The solid-phase was also fixed with zinc acetate (20 %) and S^0 was extracted overnight in a mixture of methanol and toluene (FisherScientific) (3:1). The liquid phase was removed after centrifugation and the radioactivity of S^0 in the extract was measured. Notably, this procedure would split polysulphides, so that the S(-II) would be fixed as ZnS and the S^0 would be extracted with the toluene methanol mixture. The remaining solid-phase was then sequentially distilled following the method of (Fossing and Jørgensen, 1989) in order to separate the acid volatile sulphides (AVS, mostly FeS) from the chromium reducible sulphur (CRS, mostly pyrite). The evolved sulphide was trapped as ZnS and the radioactivity was measured in each of these pools. Dilutions were accounted for by weight and used to calculate the total radioactivity in each pool.

In addition to the measurements of radioactivity, the concentration of each sulphur pool was quantified as follows. Sulphide fixed as ZnS (porewater sulphide, AVS and CRS) was measured spectrophotometrically (Cline, 1969). SO_4^{2-} was quantified by ion chromatography on a Dionex system utilizing an AG-18/AS-18 column with a KOH eluent

after Pellerin et al. (2018). Extracted S^0 was measured using reverse-phase HPLC (Thermo-Fischer) after the method of (Yücel et al., 2010), using a C-18 column and 98% methanol 2% water eluent, with detection at 230 nm. Standard solutions were prepared by dissolving S_8 in 3:1 methanol toluene.

Sulphate reduction rates were measured parallel to the sulphide oxidation rate measurements in sediment from the same core. After sediment homogenisation as described above, 5 mL sediment was incubated with $^{35}SO_4^{2-}$ in syringes after the method of (Røy et al., 2014). The syringes were incubated at 15 °C for 24 hours and the experiment was stopped by fixing the sediment in zinc acetate and freezing it. Sulphate reduction rates were then determined after single-step distillation (Røy et al., 2014).

2.2 Sulphide oxidation rate calculations

Due to isotope exchange between reduced sulphur species, quantification of sulphide oxidation rates could only be conducted when the experiment had reached a quasi-steady-state with respect to isotope exchange, which was typically reached after 2-3 hours (Fig. 2). Sulphide oxidation rates were calculated based upon the accumulation of radioactivity in the sulphate pool within the two days of the experiment (but usually within 24 hours) after this quasi-steady-state was reached. Experiments were typically terminated after approximately 24 hours, as, after this time, larger changes in the distribution of radioactivity (Fig. 2) and fluctuating sulphide concentrations were observed in some cases, indicating that the steady-state assumption no longer held. The increase of radioactivity in CRS after 24 hours could be due to its formation from AVS, as sulphide concentrations increase or further binding of radioactive sulphide or sulphur to impurities on the pyrite surface (for example as ZnS, Fossing et al, 1992).

In order to calculate sulphide oxidation, the specific radioactivity of the porewater sulphide, which was assumed to be the reacting pool, was first determined by dividing the average radioactivity present in this pool by the concentration of sulphide in the porewater (Eq. 1).

$$(1)\ \text{Specific activity } (H_2S) = \frac{\text{Radioactivity (CPM cm - 3)}}{\text{Concentration (nmol cm - 3)}}$$

The average radioactivity for sulphide was used as this value was relatively variable (up to 50%), likely due to loss incurred during the separation procedure. The sulphide oxidation rate,

that is the conversion rate of $H_2{}^{35}S$ to $^{35}SO_4^{2-}$, was then calculated by dividing the transfer of ^{35}S from H_2S to SO_4^{2-} (e.g. the rate of $^{35}SO_4^{2-}$ increase) by the specific radioactivity of the sulphide (Eq. 2, Fig. 3).

$$(2)\ \text{Sulphide oxidation rate} = \frac{\Delta 35SO42 - /\Delta t\ (\text{CPM cm} - 3\ \text{day} - 1)}{\text{Specific activity}\ (H^2S)\ (\text{CPM nmol} - 1)}$$

This approach assumes that sulphide is the reactant and only considers sulphide oxidation that proceeds to SO_4^{2-}. Implicit in this assumption is the idea that even if the oxidation proceeds through S^0, the primary reactant was sulphide. Sulphide oxidation only to S^0 would not be detected using this method and cannot be determined by radiotracer experiments due to isotope exchange between sulphide and S^0. The error for these measurements was determined as the error associated with the linear regression used to calculate the accumulation of radioactivity in sulphate. We assume here that all measured rates (sulphide oxidation and sulphate reduction) represent gross rates, as the radioactivity of the reacting pool is high relative to the product pool. It is possible that some radioactivity produced during sulphide oxidation or sulphate reduction is returned to the reacting pool, however we assume that the uncertainty associated with such parallel reactions is less than the uncertainty with the method itself (i.e. associated with determining slopes and with respect to sediment heterogeneity).

2.5 Iron reactivity experiments

The amount and the reactivity of Fe(III) in the sediment were determined with the continuum reactivity approach (Postma, 1993) with time-course extraction experiments using bicarbonate-buffered citrate-ascorbate (20 g/L (+)-sodium L-ascorbate, crystalline, ≥98%, 50 g/L Sodium bicarbonate, 50g /L Sodium citrate dihydrate, ≥99%, Sigma Aldrich) at pH 7.5 as the extractant. Ascorbate was chosen as the extractant as it has been shown to extract only the most reactive Fe(III) minerals (Reyes and Torrent, 1997; Hyacinthe et al., 2006), which would be expected to react with sulphide over a time that is relevant for the sulphide oxidation experiment (minutes to days). The reactive continuum model describes the mass-normalized rate of Fe(III) reduction (Postma, 1993, Eq. 3):

$$(3)\ \frac{J}{M_{(0)}} = \frac{v}{a}\left(\frac{M_{(t)}}{M_{(0)}}\right)^{1+\frac{1}{v}}$$

where J is the dissolution rate ($\mu mol \cdot cm^{-3} s^{-1}$), $M_{(0)}$ ($\mu mol \cdot cm^{-3}$) is the initial concentration of ascorbate extractable Fe(III) in the sediment , v/a is the apparent rate constant (s^{-1}, showing

the initial reactivity of the pure mineral phase), 1+1/v is the apparent reaction order (describing the heterogeneity of reactivities in the mineral mixture), and $M_{(t)}$ (μmol·cm^{-3}) is the corresponding mass of iron left in the sediment at time t (seconds). The time-dependent development of $M_{(t)}$ is described by Eq. 4:

$$(4)\ M_{(t)} = M_{(0)}\left(\frac{a}{a+t}\right)^{v}$$

The parameters a and v were calculated in R by applying the nls (nonlinear least squares) method with Eq. 4 to experimentally determined data. The r^2 of the fit was > 0.90. The initial rate of Fe(III) reduction per cm^3 of sediment (μmol Fe reduced·cm^{-3}·s^{-1}) was calculated by multiplying the apparent rate constant v/a with $M_{(0)}$. The initial rate reflects the oxidising capacity of the Fe(III) within the whole sediment, not only of the pure mineral phase.

Fe(II) concentrations in the extractant were determined after fixing the samples in 1 M HCl (final concentration, ACS reagent, 37% Merck) with the ferrozine assay (50% (w/v) Ammoniumacetate, Sigma Aldrich; 0.1 % (w/v) Ferrozine, FerroZine™ Iron Reagent, PDT disulfonate monosodium salt hydrate, 97%, -Sigma-Aldrich) after Stookey (1970) with a detection limit of 1 μM in 96-well microtiter plates. The absorption of the Fe(II)-ferrozine complex was determined at 562 nm in a microplate reader (FLUOstarOmega, BMG Labtech). Standards were made in 1M HCl using Fe(II)$(NH_4)2SO_4$ *$6H_2O$ (for analysis EMSURE® ISO, Sigma-Aldrich) in concentrations from 1-200 μM

3. Results

3.1 Sulphide oxidation and sulphate reduction rates

Sulphate concentrations in Aarhus Bay surface sediment at Station M5 ranged between 15 and 25 mM in the surface sediment and began to decrease from below 5 – 10 cm depth to the sulphate-methane transition zone (SMTZ) located at 60 cm. Sulphide concentrations were low in the surface sediment and increase to approximately 3 mM at the SMTZ (Pellerin et al., 2018; Table 1).

In Core A, sulphide oxidation rates up to 84 nmol·cm^{-3}·day^{-1} were measured in the surface sediment, corresponding to about 40 % of the sulphate reduction rate. However, sulphide oxidation was limited to the surface sediment (≤ 10 cm) and was below the quantification limit throughout the remainder of the sulphate zone (Fig. 4A). Sulphide

oxidation (i.e. a positive slope of $\Delta^{35}SO_4^{2-}$ over time) was also detected between 10 – 20 cm, but as the error associated with the measurement is larger than the measurement itself, the rate cannot be quantified. Sulphide oxidation activity is shown at higher resolution in the surface sediment in the second core, Core B (Fig. 4B). Sulphide oxidation rates of up to 150 $nmol \cdot cm^{-3} \cdot day^{-1}$ were determined in the top sediment layer (0 – 2 cm), corresponding to nearly twice the sulphate reduction rate in the top two centimetres of the sediment, but the rates decreased quickly with depth and could not be quantified by 6-8 cm. Sulphate reduction rates were high in the surface sediment in both cores (up to 210 $nmol \cdot cm^{-3} \cdot day^{-1}$) and generally decreased with increasing depth (Fig. 4; Table 1). The sulphate reduction rates determined here are comparable with previously measured rates from Aarhus Bay (Holmkvist et al., 2011; Pellerin et al., 2018).

3.2 Concentration and reactivity of the Fe(III) pool

Reactive Fe(III) concentrations were highest in the surface sediment (0 – 2 cm) and decreased with depth (Fig. 5A). The reactive Fe(III) pool at the surface also had the fastest initial reaction rate during the extraction compared with the deeper depths (Table 2), meaning that this pool was both larger and more reactive than the Fe(III) at the subsequent depths (Fig. 5B). Even in the deeper, more sulphidic sediment (e.g. from 10 – 16 cm depth), small quantities of reactive Fe(III) (1.6 – 0.96 $\mu mol \cdot cm^{-3}$) were extractable by the ascorbate extraction. The apparent rate constant (v/a), showing the initial reactivity of the pure mineral phase, was high for the two deepest measured sediment depths. However, compared to the surface, the heterogeneity parameter (1+1/v) was high for these samples indicating that only a smaller fraction of the iron was so highly reactive (Table 2).

Although the reactive continuum model could be fitted very well (with an R^2 of >0.97) to the dissolution curves from the samples of the top three and the two deepest sediment sections, the fit of the model to the dissolution curves of the three sediment sections between 6 and 12 cm depth was not as good (R^2 between 0.9-0.94), which led to a slight underestimation of both the initial rates and the heterogeneity in these samples.

4. Discussion

4.1 Comparison with previous estimates of sulphide oxidation rates

Sulphide is oxidized chemically with oxygen at rates that are strongly stimulated in the presence of trace metals such as Mn(II) or Fe(II) (Chen and Morris, 1972; Millero et al., 1987; Vazquez et al., 1989; Luther et al., 2011). Sulphide is also oxidized abiotically by Mn oxides (Yao and Millero, 1993) and Fe oxides (Afonso and Stumm, 1992; Yao and Miller, 1996; Poulton et al., 2004) at rates that have been determined experimentally in aqueous solution with pure mineral phases. The rate equations derived yielded rates orders of magnitude higher than those measured here, likely because those experiments did not account for the complexities of natural sediments, such as organic coatings, particles and diffusion limitation. Additionally, those experiments predominately considered the disappearance of sulphide, rather than the accumulation of SO_4^{2-} as the product, as we do, which is often not the terminal product in chemical studies. Although they yield important information related to relative reactivity and reaction mechanisms, those experimental rates cannot be directly compared to our experiments in undiluted sediments.

Experiments done with anoxic marine sediments have shown that sulphide oxidation is strongly stimulated by the addition of manganese or iron oxides (Burdige and Nealson, 1986; Aller and Rude, 1988; Canfield, 1989; King, 1990). It was thereby demonstrated that elemental sulphur is an important intermediate product and that also thiosulphate or sulphite are produced as intermediates at low concentration (Zopfi et al., 2004; Fossing and Jørgensen, 1990; Findlay and Kamyshny, 2017).

The present study is the first report of directly measured sulphide oxidation rates using ^{35}S radiotracer in unamended and undiluted sediments. Moeslund et al. (1994) used the difference between gross (total ^{35}S-measured sulphate reduction) and net (sulphate reduction less sulphide oxidation) sulphate reduction rates determined from time-course incubations of sulphate reduction rates to estimate sulphide oxidation rates in Aarhus Bay. They calculated a rate of 195 $nmol \cdot cm^{-3} \cdot day^{-1}$ for the surface sediment (0 – 1.5 cm) and of 2 $nmol \cdot cm^{-3} \cdot day^{-1}$ for deeper sediment (6 – 11 cm). Gross and net sulphate reduction rates for both depths were 250 and 55 $nmol \cdot cm^{-3} \cdot day^{-1}$ between 0 and 1.5 cm and 44 and 42 $nmol \cdot cm^{-3} \cdot day^{-1}$ between 6 and 11 cm, respectively. These calculated sulphide oxidation rates agree very well with our measured rates (Table 1), despite the methodological differences. More recently, Michaud et al. (2020) estimated sulphide oxidation in Arctic sediment based upon differences in net and gross sulphate reduction determined in bag incubation experiments from a comparison between changes in sulphate concentration over time and radiotracer sulphate reduction experiments. For surface sediment at Station J in Smeerenburgfjorden, Svalbard, which is geochemically similar to Aarhus Bay and has SRR of about 100 $nmol \cdot cm^{-3} \cdot day^{-1}$, they

estimate a sulphide oxidation rate of 55 nmol·cm^{-3}·day^{-1}, which is within the range of our values determined from directly monitoring the production of $^{35}SO_4^{2-}$. Finally, using the data presented for slurry experiments in Fig. 1 of (Fossing et al., 1992) and our Eqs. 1 and 2, we can calculate the sulphide oxidation rate from those previous experiments. In this case, the slope of accumulation of radioactivity in the sulphate pool was 470 µmol·cm^{-3}·day^{-1} and the specific activity of sulphide was 1700 CPM· µmol^{-1}. This yields a sulphide oxidation rate of 270 nmol·cm^{-3}·day^{-1}. The corresponding sulphate reduction rate was 530 nmol·cm^{-3}·day^{-1}. Those experiments were conducted using sediment from Kysing Fjord, where rates are generally higher than in Aarhus Bay.

4.2 The role of Fe in driving sulphide oxidation

The distribution of sulphide oxidation rates in the sediment correlates well with the distribution of reactive Fe(III) in the sediments of Aarhus Bay. Although oxygen is depleted within the top millimetres of the sediment and manganese oxides within the top 1.5 cm (Thamdrup et al., 1994), reactive iron oxides persist throughout the surface bioturbated sediment (Fig. 5) and are likely the predominant oxidant for sulphide in our experiments. Organic matter can also act as an oxidant for sulphide (Heitmann and Blodau, 2006; Yu et al., 2015); however, as organic matter was not characterised in this study, our discussion is limited to inorganic oxidants.

The preponderant product of sulphide oxidation by Fe oxides is elemental sulphur, both in the experimental studies discussed above in section 4.1 and in qualitative studies of sulphide oxidation in sediments (Aller and Rude, 1988; King, 1990; Böttcher et al., 2001). However, although Fe oxides likely constitute the main oxidant and are expected to produce S^0 as the predominant product, our experimental procedure determined sulphide oxidation rates only from the accumulation of radiotracer in SO_4^{2-}. The complete oxidation of sulphide to sulphate may indicate the contribution from microorganisms in the sediment, through mediating a direct oxidation or through disproportionation of elemental sulphur, as sulphide concentrations in the surface sediment are below the thermodynamic threshold for S^0 disproportionation. Disproportionation of elemental sulphur to form sulphate is thermodynamically unfavourable at sulphide concentrations greater than 1 mM (Thamdrup et al., 1993). This means that the formation of sulphate via microbial sulphur disproportionation is possible down to about 20 cm depth; however, if this is the case, the process proceeds at

rates that are too low to detect below the surface sediment with our method. The sulphide oxidation activity that is measured in these incubation experiments is that which occurs on relatively short timescales of hours to days. The determination of sulphide oxidation rates by our method is dependent upon the slope of radioactive sulphate production. Our ability to determine the slope is then dependent upon the strength of the signal (i.e. the slope of the accumulation of radioactivity in the SO_4^{2-} pool) relative to the background (background radioactivity in the SO_4^{2-} pool). As both signal and background increase by the same proportion by the addition of more radioactivity, this would not change the detection limits. With depth, the intensity of the signal to background ratio decreases due to slower rates and increasing sulphide concentration, which lowers the specific activity of the sulphide and dilutes the radiotracer, thereby decreasing the sensitivity of the method.

It is likely that sulphide oxidation persists throughout the sulphate reduction zone due to reaction with less reactive Fe minerals, but that this oxidation proceeds mostly to elemental sulphur, which would be undetectable by our method. Interestingly, in Core B, we lose detection of sulphide oxidation at about 8 cm below the seafloor, which, at our sampling resolution, is the depth at which sulphide concentrations increase an order of magnitude and the ratio of iron to sulphide subsequently decreases significantly (Table 1). This may explain the loss of detection, as the oxidant to sulphide ratio has been linked to the primary product formation, with sulphate and oxyanions forming at high ratios, and elemental sulphur forming at low ratios (Chen and Morris, 1972). Indeed, elemental sulphur concentrations peak in the surface sediment at M5 and there are low amounts of S^0 present down to about 60 cm at M5, indicative either of sulphide oxidation or the burial and consumption of S^0 from the surface sediment (Pellerin et al., 2018).

There is gradual accumulation of CRS with depth at M5, which indicates that some of the buried iron reacts with sulphide and elemental sulphur to form pyrite on timescales of the hundreds of years over which the sediment was deposited; however, based on the sulphur isotope composition of pyrite in a nearby station in Aarhus Bay (Station M24, Pellerin et al., 2018), as well as its depth distribution, most is formed while the sediment was still near the surface (see Section 4.3). This seems to indicate that even on longer timescales, iron is relatively non-reactive and the extent of sulphide oxidation is limited below the bioturbation zone. Most of the observed S^0 was thus formed at the surface and was buried and slowly consumed with depth, for example to form pyrite (Luther, 1991). Such a limitation of

sulphide oxidation due to low iron reactivity is consistent with the iron extractions, which demonstrate that highly reactive iron is nearly depleted within the bioturbation zone.

Raiswell and Canfield (1996) divide sedimentary Fe content roughly into two pools, based on reactivity: (1) A pool of iron oxides that reacts with sulphide within months and (2) Fe bearing silicates that react with sulphide over thousands of years. As even less reactive Fe oxides such as hematite and goethite react with sulphide over timescales of weeks to months (Poulton et al., 2004), they would therefore be depleted quickly below the bioturbated layer; thus most Fe buried in the sulphidic sediment below the bioturbation zone is likely present in silicate minerals. The half-life of sulphide reacting with iron in silicate minerals as determined by (Canfield et al., 1992) for sediment from the Long Island Sound is on the order of 100,000 years, which is notably faster than that determined for much older sediments on the Peru Margin (5.3 million years, Raiswell and Canfield, 1996), indicating variable reactivities even within the silicate-bound iron pool. The sediment age at the lower boundary of the SMTZ at Station M5 is 700 years (Rasmussen et al., 2018). Using the rates of Fe silicate reaction with sulphide determined by Raiswell and Canfield (1996), the rate of sulphide oxidation to sulphate would be 0.91 $nM \cdot yr^{-1}$. Assuming that the Fe buried in Aarhus Bay has a similar reactivity towards sulphide, 0.63 µM sulphate could be produced in 700 years. New estimates of sulphate concentrations below the SMTZ are as low as 5 µM, which is still an order of magnitude higher than this estimate, despite measurable sulphate reduction below the SMTZ (Pellerin et al., 2018). This indicates that the iron minerals present likely have a higher reactivity than those in the studies of (Canfield et al., 1992) and Raiswell and Canfield, 1996), or that small amounts of sulphide may be oxidised during porewater sampling.

4.3 Sulphur oxidation and burial in marine sediments

The combined burial and oxidation of sulphur and organic matter in marine sediments controls Earth's climate and atmospheric oxygen levels over geological timescales (Berner et al., 2000) and will depend upon the relative rates of sulphide oxidation and organic matter oxidation. In coastal and shelf sediments, sulphate reduction to sulphide appears to be the prevailing processes for anaerobic organic matter oxidation (Jørgensen 1982); thus, sulphate reduction rates are a proxy for organic matter decomposition throughout the sulphate zone.

As the majority of sulphide oxidation and pyrite formation occurs in the surface sediment, the amount of sulphur that is buried or lost from the sediment through diffusion or

oxidation will depend upon the amount and reactivity of iron in the surface sediment. Particularly at the very surface, oxygen supplied by diffusion, advection and bioturbation keeps the sedimentary Fe oxidised. The sulphide oxidation potential of the top layer of the surface sediments (0 – 2 cm) in Aarhus Bay was greater than the production rate of sulphide in those sediments, based upon sulphate reduction rate experiments, so that this sediment layer represents a net sink for sulphide. In contrast, all subsequent layers represented a net source of sulphide, as the sulphide production rates (i.e. sulphate reduction rates) were greater than the oxidation rates.

To loosely approximate the magnitude of different rates for sulphur in the surface sediment, we can compare the rates of sulphide production through sulphate reduction and the loss of sulphide through oxidation. The summed sulphate reduction rate for the top 0-6 cm at M5, based upon the rate measurements in Core B, is 283 $nmol \cdot cm^{-2} \cdot day^{-1}$ and the summed sulphide oxidation rate is 259 $nmol \cdot cm^{-2} \cdot day^{-1}$, meaning that within the top 6 cm of the sediment, most of the produced sulphide was reoxidised to sulphate, which agrees well with previous mass balance calculations (Jørgensen, 1982). However, when the top 10 cm are considered, only about two thirds of the produced sulphide is reoxidised to sulphate, due to the faster decrease in sulphide oxidation relative to sulphate reduction.

In addition to the sulphide that is oxidised, pyrite accumulates to about 75 $\mu mol \cdot cm^{-3}$ by 6 cm at Station M5 (Pellerin et al., 2018); an average rate of 1.25 $\mu mol \cdot cm^{-3} \cdot yr^{-1}$. The cumulative rate for the 0-6 cm depth interval is thus 7.5 $\mu mol\ cm^{-2}\ yr^{-1}$ or 20 $nmol\ cm^{-2}\ d^{-1}$, which corresponds to approximately a tenth of the total sulphide produced from sulphate reduction. S^0 accumulation is about an order of magnitude lower, and sulphur is also present as AVS, or may be lost from the system due to diffusion. In the deeper sediment, in which sulphide oxidation drops below our detection limit (6 – 60 cm), pyrite slowly increases from about 75 to 110 $\mu mol \cdot cm^{-3}$, corresponding to an average formation rate of 0.07 $\mu mol \cdot cm^{-3} \cdot yr^{-1}$; nearly two orders of magnitude lower than the rates in the surface sediment, reflecting the decreasing reactivity of iron between the surface and deeper sediment, where Fe reacts with sulphide over timescales of hundreds to thousands of years.

These calculations should be taken only as a first approximation of the relative magnitude of these processes in our experiments, due to experimental uncertainty, sediment heterogeneity and omission of processes such as organic sulphur formation and diffusion of

sulphide from the sediment. However, the patterns that we observe are likely common to marine sediments with similar biogeochemical characteristics.

5. Conclusions

Sulphide oxidation rates were up to twice sulphate reduction rates in the oxidised surface sediment and decreased to below detection under the top 10 – 20 cm. Sulphide oxidation rates appear to be driven by the reactivity of Fe oxides, demonstrated by the correlation between the reactivity of ferric iron minerals within the sediment and zones of active sulphide oxidation and the prevalence of Fe over other oxidants (O_2, NO_3^-, Mn). Although Fe oxide minerals are likely the primary oxidant for sulphide, sulphate is observed as the final product in the surface 6 cm, indicating a potential role for microorganisms in mediating the oxidation, perhaps through disproportionation of elemental sulphur. Below 8 cm, sulphide oxidation rates were too low to be quantified with our experimental method, which is likely related to the drop in iron reactivity and iron to sulphide ratio. Such a decrease in Fe reactivity is further evidenced by a 20-fold decrease in pyrite formation rates between the top 6 centimetres and 6 – 60 cm depth. These results have environmental implications in both the short and longer-term, as the amount and reactivity of iron will control the release of sulphide from sediments underlying anoxic and hypoxic waters to the water column, where it is toxic to fish and other aerobic organisms. On geological timescales, the burial of S as pyrite impacts atmospheric CO_2 and O_2 concentrations.

Acknowledgments

Kasper Kjeldsen and Hans Røy are thanked for collecting the sediment cores. This work was supported by a Marie-Curie European Fellowship [SedSulphOx, MSCA 746872] to AJF. KL acknowledges support from the Deutsche Forschungsgemeinschaft [DFG 389371177]. BBJ acknowledges support from an ERC Advanced Grant (MICROENERGY, grant #294200, EU 7th FP), the Danish National Research Foundation (DNRF grant #104), and the Danish Council for Independent Research (DFF – 7014-00196).

Research Data

Research Data associated with this article are included as electronic annexe. Electronic Annex 1 contains the raw data used in the sulphide oxidation calculations. Electronic Annex 2 includes plots of the sulphate radioactivity data used in the rate calculations.

Data Availability

All data not included in the tables and figures in the manuscript are included in the electronic annexe.

References

Aller R. C. and Rude P. D. (1988) Complete oxidation of solid phase sulfides by manganese and bacteria in anoxic marine sediments. *Geochim. Cosmochim. Acta* **52**, 751–765.

Arnold G. L., Brunner B., Müller I. a and Røy H. (2014) Modern applications for a total sulfur reduction distillation method - what's old is new again. *Geochem. Trans.* **15**, 4.

Berner R. A., Smith M. D., Pearl J. C., Conrath B. J., Christensen P. R. and Res J. G. (2000) Isotope Fractionation and Atmospheric Oxygen : Implications for Phanerozoic O_2 Evolution. *Res, J Geophys* **287**, 1630–1634.

Beulig F., Røy H., McGlynn S. E. and Jørgensen B. B. (2019) Cryptic CH_4 cycling in the sulfate-methane transition of marine sediments apparently mediated by ANME-1 archaea. *ISME J.* **13**, 250-262.

Böttcher M. E., Thamdrup B. and Vennemann T. W. (2001) Oxygen and sulfur isotope fractionation during anaerobic bacterial disproportionation of elemental sulfur. *Geochim. Cosmochim. Acta* **65**, 1601–1609.

Bottrell S. H. and Newton R. J. (2006) Reconstruction of changes in global sulfur cycling from marine sulfate isotopes. *Earth-Science Rev.* **75**, 59–83.

Brenner H., Braeckman U., Guitton M. Le and Meysman F. J. R. (2016) The impact of sedimentary alkalinity release on the water column CO_2 system in the North Sea. , 841–863.

Brüchert V. (1998) Early diagenesis of sulfur in estuarine sediments: The role of sedimentary humic and fulvic acids. *Geochim Chemochin Acta* **62**, 1567-1586.

Burdige D. J. and Nealson K. H. (1986) Chemical and microbiological studies of sulfide mediated manganese reduction. *Geomicrobiol. J.* **4**, 361–387.

Canfield D. E. (1989) Reactive iron in marine sediments. *Geochim. Cosmochim. Acta* **53**, 619–632.

Canfield D. E., Raiswell R. and Bottrell S. H. (1992) The reactivity of sedimentary iron minerals toward sulfide. *Am. J. Sci.* **292**, 659–683.

Chen K. and Morris J. (1972) Kinetics of oxidation of aqueous sulfide by O_2. *Environ. Sci. Technol.* **6**, 529–537.

Chen X. H., Andersen T. J., Morono Y., Inagaki F., Jørgensen B. B. and Lever M. A. (2017) Bioturbation as a key driver behind the dominance of Bacteria over Archaea in near-surface sediment. *Sci. Rep*. **7**, 2400.

Cline J. (1969) Spectrophotometric Determination of Hydrogen Sulfide in Natural Waters. *Limnol. Oceanogr.* **14**, 454–458.

dos Santos Afonso M. and Stumm W. (1992) Reductive dissolution of iron (III)(hydr) oxides by hydrogen sulfide. *Langmuir*, 1671–1675.

Fike D. A., Bradley A. S. and Rose C. V. (2013) Rethinking the Ancient Sulfur Cycle. *Annu. Rev. Earth Planet. Sci.* **43**, 593–622.

Findlay A. J. and Kamyshny A. (2017) Turnover Rates of Intermediate Sulfur Species (S_x^{2-}, S^0, $S_2O_3^{2-}$, $S_4O_6^{2-}$, SO_3^{2-}) in Anoxic Freshwater and Sediments. *Front. Microbiol.* **8**.

Finster K. (2008) Microbiological disproportionation of inorganic sulfur compounds. *J. Sulfur Chem.* **29**, 281–292.

Fossing H. and Jørgensen B. B. (1989) Chromium Reduction Method of bacterial sulfate reduction in sediments: Measurement reduction of a single-step chromium method Evaluation. *Biogeochemistry* **8**, 205–222.

Fossing H. and Jørgensen B. B. (1990) Isotope Exchange-Reactions with Radiolabeled Sulfur-Compounds in Anoxic Seawater. *Biogeochemistry* **9**, 223–245.

Fossing H., Thode-Andersen S. and Jørgensen B. (1992) Sulfur isotope exchange between 35 S-labeled inorganic sulfur compounds in anoxic marine sediments. *Mar. Chem.* **38**, 117–132.

Froelich P. N., Klinkhammer G. P., Bender M. L., Luedtke N. A., Heath G. R., Cullen D., Dauphin P., Hammond D. and Hartman B. (1979) Early oxidation of organic matter in pelagic sediments of the eastern equatorial Atlantic: suboxic diagenesis. *Geochim. Cosmochim. Acta* **43**, 1075–1090.

Glombitza C., Pedersen J., Røy H. and Jørgensen B. B. (2014) Direct analysis of volatile fatty acids in marine sediment porewater by two-dimensional ion chromatography-mass spectrometry. *Limnol.Oceanogr.: Meth*. **12**, 455-468.

Habicht K. S., Gade M., Thamdrup B. and Berg P. (2002) Calibration of Sulfate Levels in the Archean Ocean. *Science* **298**, 2372-2374.

Hansen J. W., Thamdrup B. and Jørgensen B. B. (2000) Anoxic incubation of sediment in gas-tight plastic bags: A method for biogeochemical process studies. *Mar. Ecol. Prog. Ser.* **208**, 273–282.

Heitmann T. and Blodau C. (2006) Oxidation and incorporation of hydrogen sulfide by

dissolved organic matter. *Chem Geol*. **235**, 12-20.

Henneke E., Luther G. W., De Lange G. J. and Hoefs J. (1997) Sulphur speciation in anoxic hypersaline sediments from the eastern Mediterranean Sea. *Geochim. Cosmochim. Acta* **61**, 307–321.

Holmkvist L., Ferdelman T. G. and Jørgensen B. B. (2011) A cryptic sulfur cycle driven by iron in the methane zone of marine sediment (Aarhus Bay, Denmark). *Geochim. Cosmochim. Acta* **75**, 3581–3599.

Holmkvist L., Kamyshny A., Bru V., Ferdelman T. G. and Jørgensen B. B. (2014) Sulfidization of lacustrine glacial clay upon Holocene marine transgression (Arkona Basin , Baltic Sea). *Geochim. Cosmochim. Acta* **142**, 75-94.

Hyacinthe C., Bonneville S. and van Cappellen P. (2006) Reactive iron(III) in sediments: Chemical versus microbial extractions. *Geochim Cosmochim Acta* **70**, 4166–4180.

Jamieson J. W., Wing B.A., Farquhar J. and Hannington M. D. (2013) Neoarchaean seawater sulphate concentrations from sulphur isotopes in massive sulphide ore. *Nat. Geosci* **6**, 61–64.

Jochum L., Chen X., Lever M. A., Loy A., Schreiber L., Jørgensen B. B., Schramm A. and Kjeldsen K. U. (2017) Depth distribution and assembly of sulfate-reducing microbial communities in marine sediment. *Appl. Environ. Microbiol*. **83**, e01547-17.

Johnston D. T. (2011) Multiple sulfur isotopes and the evolution of Earth's surface sulfur cycle. *Earth-Science Rev.* **106**, 161–183.

Jørgensen B. B. (1982) Mineralization of organic matter in the sea bed - the role of sulphate reduction. *Nature* **296**, 643–645.

Jørgensen B. B. and Nelson D. C. (2004) Sulfide oxidation in marine sediments : Geochemistry meets microbiology. *Geol. Soc. Am. Spec. Pap. 2004* **379**, 63–81.

Jørgensen B., Bang M. and Blackburn T. (1990) Anaerobic mineralization in marine sediments from the Baltic Sea-North Sea transition. *Mar. Ecol. Prog. Ser.* **59**, 39–54.

King G. M. (1990) Effects of added manganic and ferric oxidson sulfate reduction and sulfide oxidation in intertidal sediments. *FEMS Microbiol. Ecol.* **73**, 131–138.

Langerhuus A. T., Røy H., Lever M. A., Inagaki F., Morono Y., Jørgensen B. B. and Lomstein B. Aa (2012) Endospore abundance and D:L-amino acid modeling of bacterial turnover in Holocene marine sediment (Aarhus Bay). *Geochim. Cosmochim. Acta* **99**, 87-99.

Laufer K., Nordhoff M., Røy H., Schmidt C., Behrens S., Jørgensen B. B. and Kappler A. (2016) Co-exsistence of microaerophilic, nitrate-reducing, and phototrophic Fe(II)-

oxidizers and Fe(III)-reducers in two geochemically distinct coastal marine sediments. *Appl. Environ. Microbiol.* **82**, 1433-1447.

Luther G. W. (1991) Pyrite synthesis via polysulfide compounds. *Geochim. Cosmochim. Acta* **55**, 2839–2849.

Luther G. W., Findlay A. J., MacDonald D. J., Owings S. M., Hanson T. E., Beinart R. A. and Girguis P. R. (2011) Thermodynamics and kinetics of sulfide oxidation by oxygen: A look at inorganically controlled reactions and biologically mediated processes in the environment. *Front. Microbiol.* **2**, 1–9.

Luther G. W., Ma S., Trouwborst R., Glazer B., Blickley M., Scarborough R. W. and Mensinger M. G. (2004) The roles of anoxia, H_2S, and storm events in fish kills of dead-end canals of Delaware inland bays. *Estuaries* **27**, 551–560.

Lyons T. W., Reinhard C. T. and Planavsky N. J. (2014) The rise of oxygen in Earth's early ocean and atmosphere. *Nature* **506**, 307–15.

Millero, F. J., Hubinger, S., Fernandez, M., and Garnett, S. (1987). Oxidation of H2S in seawater as a function of temperature, ph, and ionic strength. *Environ. Sci. Technol.* **21**, 439–443.

Moeslund L., Thamdrup B. and Jørgensen B. B. (1994) Sulfur and iron cycling in a coastal sediment: Radiotracer studies and seasonal dynamics. *Biogeochemistry* **27**, 129–152.

Pellerin A., Antler G., Røy H., Findlay A., Beulig F., Scholze C., Turchyn A. V and Jørgensen B. B. (2018) The sulfur cycle below the sulfate-methane transition of marine sediments. *Geochim Cosmochim Acta* **239**, 74–89.

Postma D. (1993) The reactivity of iron oxides in sediments: A kinetic approach. *Geochim. Cosmochim. Acta* **57**, 5027–5034.

Poulton S. W., Krom M. D. and Raiswell R. (2004) A revised scheme for the reactivity of iron (oxyhydr)oxide minerals towards dissolved sulfide. *Geochim. Cosmochim. Acta* **68**, 3703–3715.

Raiswell R. and Canfield D. E. (1996) Rates of reaction between silicate iron and dissolved sulfide in Peru Margin sediments. **60**, 2777–2787.

Rasmussen P., Pantopoulos G., Jensen B. J. and Olsen J. (2018) Holocene sedimentary and environmental development of Aarhus Bay, Denmark: multi-proxy evidence and regional context. *Boreas*. doi:10.1111/bor.12408

Raven M.R., Sessions A.L., Fischer W.W., Adkins J.F. (2016) Sedimentary pyrite $\delta^{34}S$ differs from porewater sulfide in Santa Barbara Basin: Proposed role of organic sulfur. *Geochim Cosmochim Acta* **186**, 120–134.

Reyes I. and Torrent J. (1997) Citrate-Ascorbate as a highly selective extractant for poorly crystalline iron oxides. *Soil Sci Soc Am J* **61**, 1647–1654.

Rickard D. and Luther G. W. (2007) Chemistry of iron sulfides. *Chem. Rev.* **107**, 514–562.

Røy H., Weber H. S., Tarpgaard I. H., Ferdelman T. G. and Jørgensen B. B. (2014) Determination of dissimilatory sulfate reduction rates in marine sediment via radioactive 35S tracer. *Limnol. Oceanogr. Methods* **12**, 196–211.

Stookey, L. L. (1970) Ferrozine - a New Spectrophotometric Reagent for Iron. *Anal. Chem.* **42**, 779–781.

Thamdrup B., Finster K., Hansen J. W. and Bak F. (1993) Bacterial disproportionation of elemental sulfur coupled to chemical reduction of iron or manganese. *Appl. Environ. Microbiol.* **59**, 101–108.

Thamdrup B., Fossing H., Jorgensen B. B. and Jørgensen B. B. (1994) Manganese, iron and sulfur cycling in a coastal marine sediment, Aarhus Bay, Denmark. *Geochim. Cosmochim. Acta* **58**, 5115–5129.

Thamdrup B, Finster K, Fossing H, Hansen J.W, Jørgensen B.B. (1994b) Thiosulfate and sulfite distributions in porewater of marine sediments related to manganese, iron, and sulfur geochemistry. *Geochim Cosmochim Acta* **58**, 67–73.

Thode-Andersen S. and Jørgensen B. B. (1989) Sulfate reduction and the formation of ^{35}S-labeled FeS, FeS_2, and S^0 in coastal marine sediments. *Limnol. Oceanogr.* **34**, 793–806.

Troelsen H. and Jørgensen B. B. (1982) Seasonal dynamics of elemental sulfur in two coastal sediments. *Estuar. Coast. Shelf Sci.* **15**, 255–266.

Vazquez, F. G, Zhang, J., and Millero, F. J. (1989). Effect of metals on the rate of the oxidation of H_2S in seawater. *Geophys. Res. Lett.* **16,** 1363–1366.

Wu, J., Boyle, E.A. (1998) Determination of iron in seawater by high resolution isotope dilution inductively coupled plasma mass spectrometry after $Mg(OH)_2$ coprecipitation. *Analytica Chimica Acta* **367**, 183–191.

Wurgarft E., Findlay A. J., Viderovich H., Herut B. and Sivan O. Sulfate reduction rates in the sediments of the Mediterranean continental shelf from combined dissolved inorganic carbon and total alkalinity profiles. *Mar. Chem.* **211**, 64-74.

Yao W. and Miller F. J. (1996) Oxidation of hydrogen sulfide by hydrous Fe (III) oxides in seawater. *Mar. Chem.* **52**, 1–16.

Yao W. and Millero F. J. (1993) The rate of sulfide oxidation by δMnO_2 in seawater. *Geochim. Cosmochim. Acta* **57**, 3359–3365.

Yu Z., Peiffer S., Göttlicher J., Knorr K. (2015) Electron Transfer Budgets and Kinetics of

Abiotic Oxidation and Incorporation of Aqueous Sulfide by Dissolved Organic Matter. *Environ Sci Tech* **49**, 5441-5449.

Yücel M., Konovalov S. K., Moore T. S., Janzen C. P. and Luther G. W. (2010) Sulfur speciation in the upper Black Sea sediments. *Chem. Geol.* **269**, 364–375.

Zopfi J., Ferdelman T. G. and Fossing H. (2004) Distribution and fate of sulfur intermediates - sulfite, tetrathionate, thiosulfate and elemental sulfur - in marine sediments. *Spec. Pap. Geol. Soc. Am.* **379**, 17–34.

Figure 1: Sampling and separation scheme for the determination of concentration and radioactivity of the different sulphur pools.

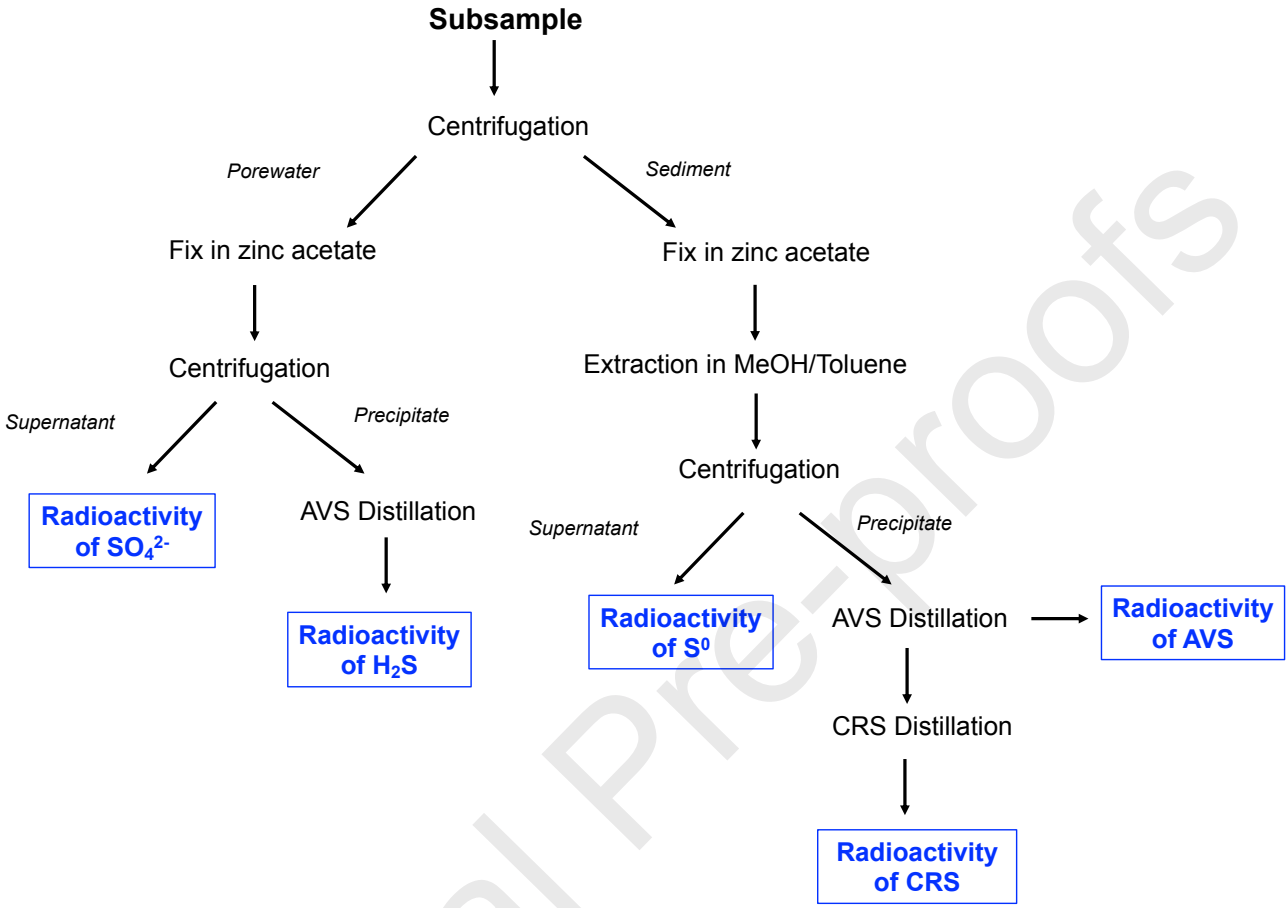

Figure 2: Timecourse of normalised radioactivity in each of the measured sulphur pools for sediment from 0-5 cm. A quasi-steady-state (e.g. low changes between the radioactivity of the respective sulphur pools) is reached after about 2 hours. After 20 hours, the radioactivity in the different pools changes slightly more (about 10%), which impacts the uncertainty associated with measurements at longer time points. Note that sulphide is plotted on a second, expanded y axis.

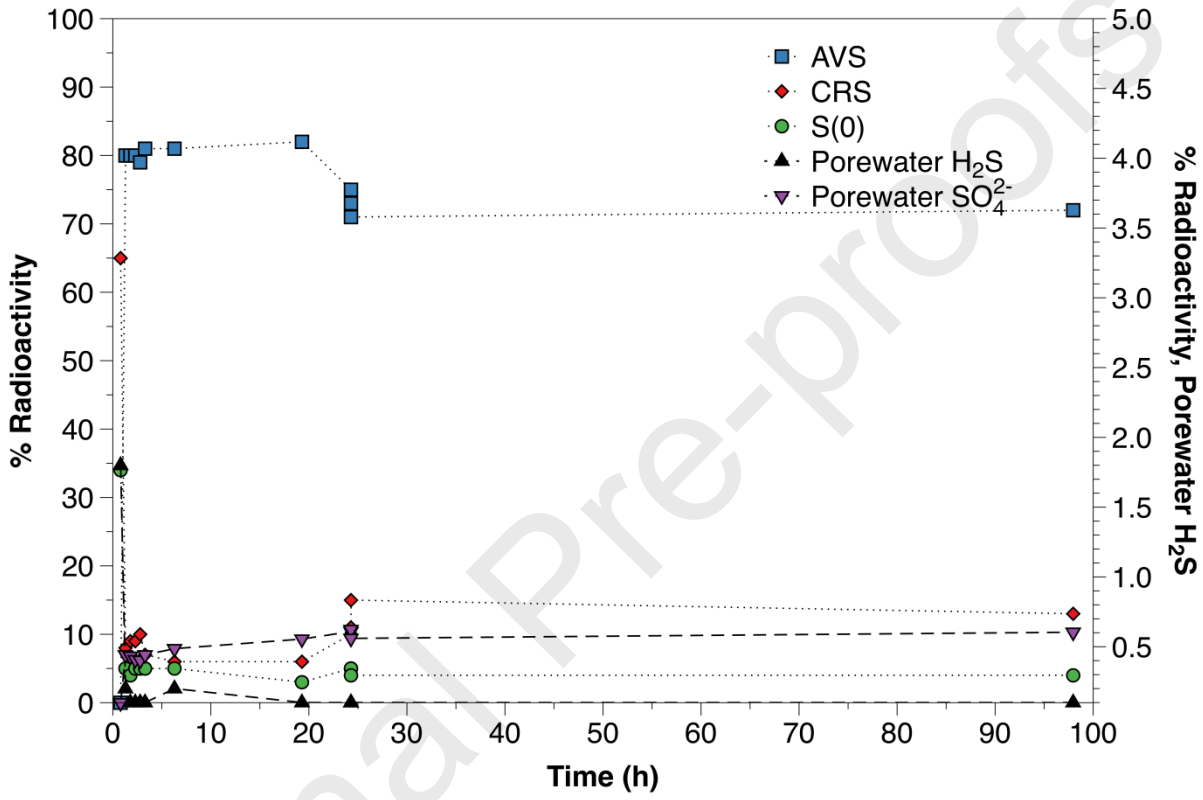

Figure 3: Accumulation of radioactivity in the sulphate pool (slope = 47, $R^2 = 0.96$) and the average specific activity of sulphide (thick grey line) throughout the time course for sediment from 0-2 cm depth in Core B. For further examples, please see Electronic Annex 2.

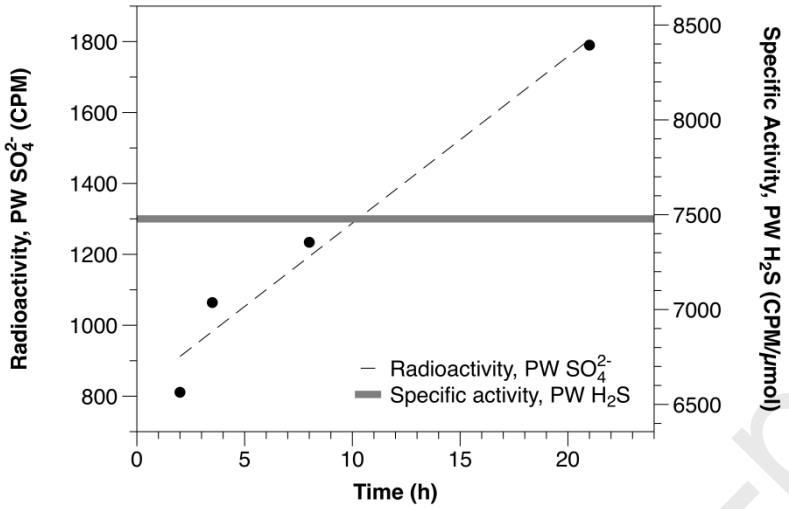

Figure 4: Sulphate reduction rates and sulphide oxidation rates (A) throughout the sediment column of Core A and (B) in the surface sediment of Core B. Note that although sulphide oxidation rates were detected and are plotted for 10 – 20 cm (Core A) and 6 – 8 cm (Core B), these values are not quantifiable. Note the differences in sampling depth resolution between then two cores. The error for the sulphide oxidation rate was determined as the error associated with the linear regression used to calculate the accumulation of radioactivity in sulphate (see methods). Error for sulphate reduction rates is from three replicate measurements.

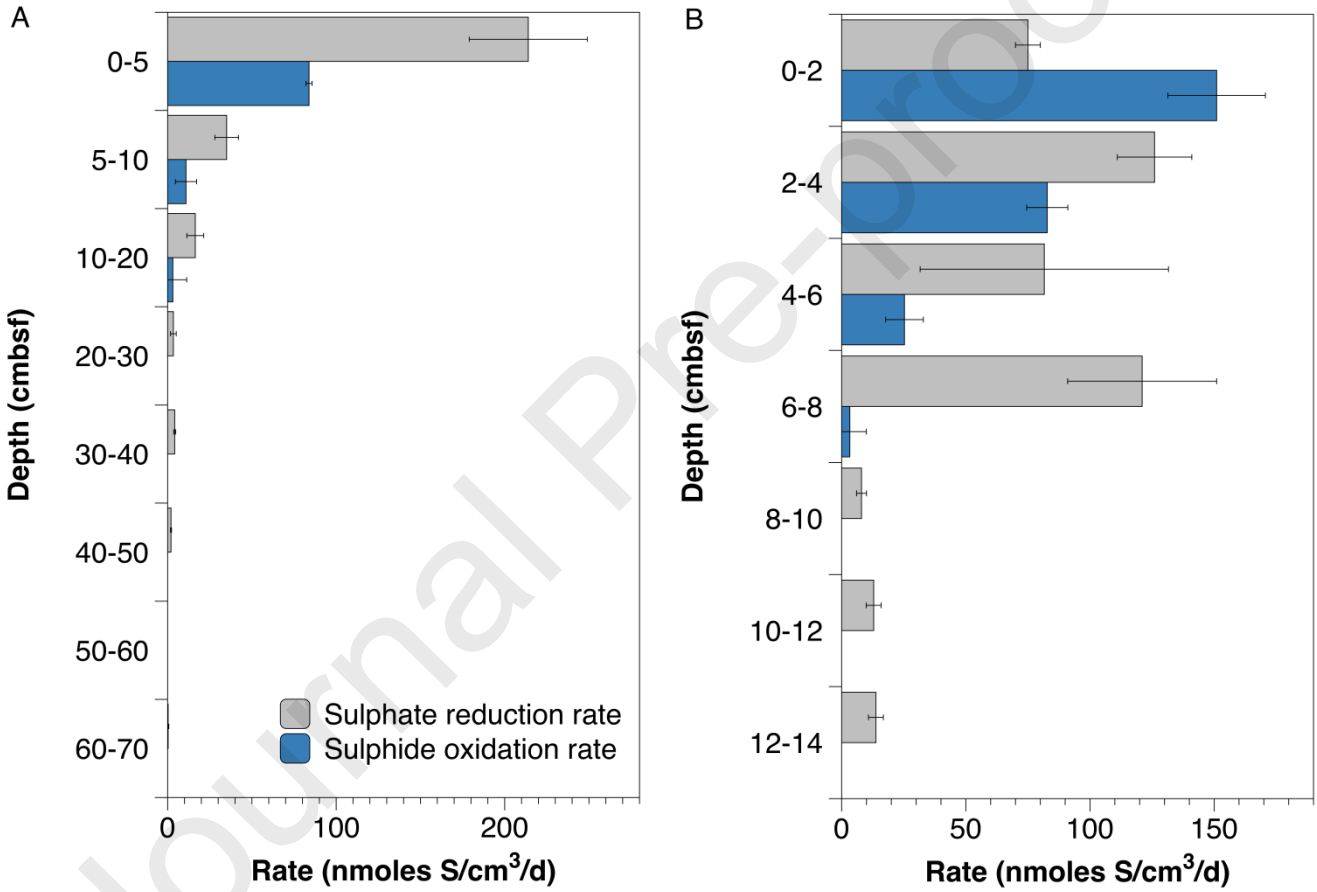

Figure 5: (A) Concentration of reactive Fe(III) and (B) dissolution curves from the time-course Fe extractions for each depth in the surface sediment (0 – 14 cm, top panel) and a zoomed in detail of the reactivity in the deeper sediment (6 – 14 cm, bottom panel). The dotted line represents the model fit.

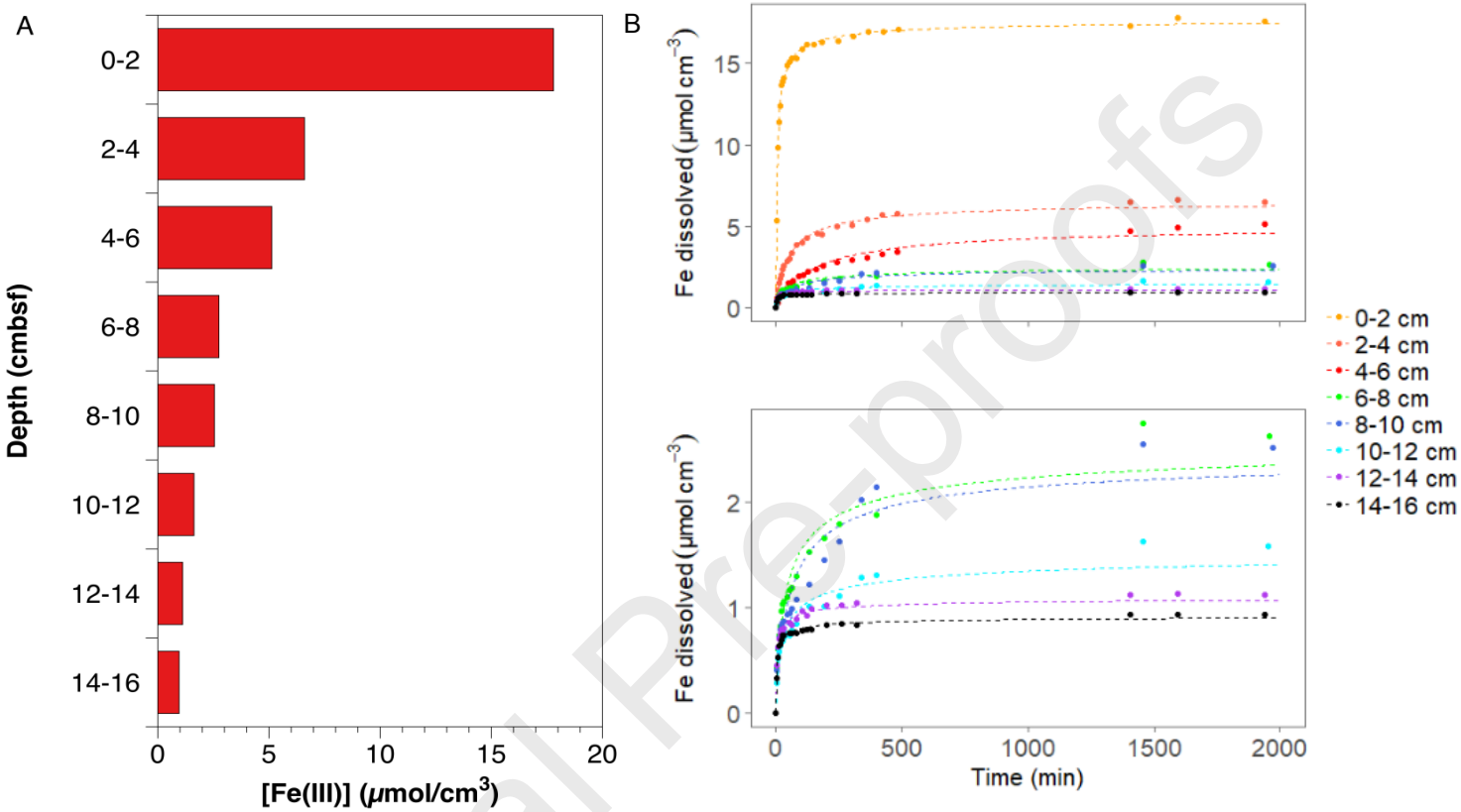

Table 1: Sulphur, iron and rate data for each of the two sediment cores. Core A is the 70 cm core, Core B is the shorter 16 cm core. F_{ox} is the fraction of the sulphate reduction rate that is reoxidised and the Fe reduction rate is the amount of iron that would be reduced, if all sulphide oxidation is due to Fe reduction. +/- indicates error on the sulphide oxidation rate. BDL = below detection limit, -- indicates that no measurement was made. *Indicates that the measurement is not quantifiable.

Depth	$[SO_4^{2-}]$ (mM)	$[\sum H_2S]$ (µmol cm^{-3})	Sulphate reduction rate (nmol $cm^{-3}day^{-1}$)	Sulphide oxidation rate (nmol $cm^{-3}day^{-1}$)	+/-	f_{ox}	[Fe(III)] (µmol cm^{-3})	Fe reduction rate (µmol $cm^{-3}day^{-1}$)	Fe:H_2S
Core A:									
0-5	24	0.053	210	84	1.8	0.4	--	--	--
5-10	26	0.18	35	11	6.3	0.3	--	--	--
10-20	22	0.40	16	3.1*	8.2	0.2	--	--	--
20-30	15	0.50	3.4	BDL	--	--	--	--	--
30-40	9.2	1.3	4.2	BDL	--	--	--	--	--
40-50	3.5	2.1	2.0	BDL	--	--	--	--	--
50-60	0.40	3.2	BDL	BDL	--	--	--	--	--
60-70	0.070	1.5	0.30	BDL	--	--	--	--	--
Core B:									
0-2	15	0.0050	75	150	20	2	17.8	1.2	3700
2-4	16	0.020	130	83	8.3	0.66	6.60	0.66	330
4-6	13	0.046	82	25	7.6	0.3	5.13	0.20	110
6-8	14	0.038	120	3.3*	6.6	0.03	2.75	0.03	73
8-10	6.0	0.28	8.0	BDL	--	--	2.55	0.025	9
10-12	7.3	0.45	13	BDL	--	--	1.63	0.016	4
12-14	7.6	0.42	14	BDL	--	--	1.12	0.011	3
14-16	--	--	--	--	--	--	0.96	0.009	--

Table 2: Fe reactivity parameters. $M_{(0)}$ is the amount of reducible Fe(III) present in the sediment. The apparent rate constant v/a equals the mass-normalized initial rate of reduction. The initial rate is the non-mass normalized rate of Fe(III) reduction. The heterogeneity parameter 1+1/v describes the heterogeneity of reactivities in the extracted mineral fraction.

Depth	M_0 (µmol Fe(III) cm^{-3})	v/a (s^{-1})*10000	initial rate (µmol Fe dissolved cm^{-3} s^{-1})*100	1+1/v	r^2 (of model fit)
0 – 2	17.80	40.1	7.21	2.67	0.99
2 – 4	6.60	3.44	0.23	2.41	0.99
4 – 6	5.13	1.09	0.06	2.32	0.97
6 – 8	2.75	4.87	0.13	3.59	0.94
8 – 10	2.55	3.34	0.09	3.04	0.90
10 – 12	1.63	8.45	0.14	3.86	0.92
12 – 14	1.12	62.2	0.70	3.56	0.98
14 – 16	0.96	62.7	0.59	3.30	0.99

Declaration of interests

☑ The authors declare that they have no known competing financial interests or personal relationships that could have appeared to influence the work reported in this paper.

The authors declare the following financial interests/personal relationships which may be considered as potential competing interests: